

Intrinsic Anomaly Detection for Multi-Variate Time Series

Stephan Rabanser^{*†}
University of Toronto & Vector Institute
stephan@cs.toronto.edu

Tim Januschowski^{*†}
Zalando Research
tim.januschowski@zalando.de

Kashif Rasul
Morgan Stanley
rasul.kashif@morganstanley.com

Oliver Borchert[†]
Technical University of Munich
borchero@in.tum.de

Richard Kurler
Amazon Research
kurler@amazon.com

Jan Gasthaus
Amazon Research
gasthaus@amazon.com

Michael Bohlke-Schneider
Amazon Research
bohlkem@amazon.com

Nicolas Papernot
University of Toronto & Vector Institute
nicolas.papernot@utoronto.ca

Valentin Flunkert
Amazon Research
flunkert@amazon.com

Abstract

We introduce a novel, practically relevant variation of the anomaly detection problem in multi-variate time series: *intrinsic anomaly detection*. It appears in diverse practical scenarios ranging from DevOps to IoT, where we want to recognize failures of a system that operates under the influence of a surrounding environment. Intrinsic anomalies are changes in the functional dependency structure between time series that represent an environment and time series that represent the internal state of a system that is placed in said environment. We formalize this problem, provide under-studied public and new purpose-built data sets for it, and present methods that handle intrinsic anomaly detection. These address the shortcoming of existing anomaly detection methods that cannot differentiate between expected changes in the system’s state and unexpected ones, i.e., changes in the system that deviate from the environment’s influence. Our most promising approach is fully unsupervised and combines adversarial learning and time series representation learning, thereby addressing problems such as label sparsity and subjectivity, while allowing to navigate and improve notoriously problematic anomaly detection data sets.

1 Introduction

Modern applications, appliances, or systems in the physical and virtual world are equipped with sensors that measure and monitor on the one hand the *state of a system* and its sub-components, and on the other hand the *environment* with which the system interacts. These measurements are typically captured by monitoring systems as multi-variate time series data sets. Examples can be found in the Internet-of-Things (IoT) or in the DevOps/AIOps space (Lu et al., 2009; Lohrmann and Kao, 2011; Nedelkoski et al., 2019; Li et al., 2020; Krupitzer et al., 2020). Our running example is that of a wind turbine; see Figure 1. Environmental variables correspond to ambient temperature, wind speed and direction and system variables correspond to

^{*}Equal contribution.

[†]Work done while at Amazon Research.

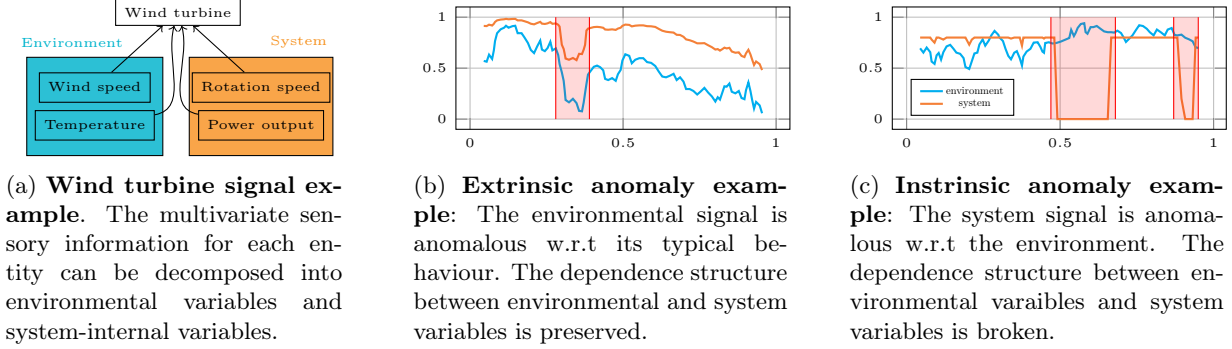


Figure 1: Structure of time series corpora (left) and different types of anomalies (middle and right).

rotator speed and internal temperature measurements, among many others. We expect internal temperature measurements to vary naturally with ambient temperature, but a deviation from the functional relationship between ambient and internal temperature measurements could point to a problem of the state of the turbine. It is this change in the functional relationship that is the principal object of interest of this work. Detecting it allows to understand deteriorations of state and health of the system independent of the environment.

To further motivate our approach, consider a simplified system where *intrinsic normality* means that a single variable y that represents the state of a system depends instantaneously on a single environmental signal x via a mapping h , i.e., we have $y = h(x) + \varepsilon$, where ε is a (not further specified) error term. We then define an *intrinsic anomaly* as a point where this functional relationship is broken, i.e. ε exceeds a threshold τ . The ideal signal to detect an intrinsic anomaly is the residual $\delta := y - h(x)$. Under normal operation this signal δ carries no information about the environmental variable x and thresholding the magnitude of this residual signal allows to define intrinsic anomalies.

We contrast intrinsic anomalies with anomalies that we would find if we considered a standard multivariate anomaly detection problem on environment variables only, which we refer to as *extrinsic anomalies*. Such problems are widely studied (see Blázquez-García et al. (2021) for a recent overview). In the wind turbine example, an extrinsic anomaly could be unexpectedly strong wind. Detecting it automatically allows to pitch out the blades if they rotate too fast. However, the pitching out of blades is not an intrinsic anomaly as it constitutes expected behaviour. Figure 1 provides an illustration of both anomaly types. Standard anomaly detection methods (Su et al., 2019a; Liu et al., 2008; Breunig et al., 2000) allow to detect extrinsic anomalies, hence we refrain from studying them further here.

The data sets for the intrinsic anomaly detection task differ from standard anomaly detection benchmarks by their division into environment and system variables. Similar to standard anomaly detection benchmarks (Bogatinovski et al., 2021; Wu and Keogh, 2021), sparsity and subjectivity of their associated labels for anomalies are practical concerns. Sparsity may be due to diverse reasons ranging from practical (e.g., data integration or cost of labelling) to fundamental (internal system failures are exceedingly rare). Subjectivity stems from the fact that failure identification often requires human insight or that alarms come from overly noisy rule-based systems (Bogatinovski et al., 2021; Wu and Keogh, 2021). Based on our practical experience, it is unrealistic to obtain a golden data set since both extrinsic and intrinsic anomalies are domain-specific and subjective. Methods for intrinsic anomaly detection should allow to iteratively improve the data. A common task is checking whether time series similar to a labelled intrinsic anomaly are labelled as such, and if not to potentially (re)label them.

The desiderata for methods for intrinsic anomaly detection are hence as follows. They need to (i) detect intrinsic anomalies and separate them from extrinsic anomalies. While an oversimplification, we will consider the problem of detection extrinsic anomaly detection as solved for the sake of this paper; (ii) sparsity of labels means that we cannot expect a supervised method to work well and instead must rely mostly on unsupervised methods; and (iii) the subjectivity of labels motivates the need for methods to facilitate human interaction with a potentially high-dimensional, complex data set in an interactive and iterative fashion (e.g., by being able to identify similar time series snippets or similar extrinsic/intrinsic anomalies). Given these desiderata, a natural choice for a method for intrinsic anomaly detection would be based on unsupervised representation

learning which enables the computation of distances in the embedding space to identify related time series interactively.

To summarize, our contributions are three-fold. First, we present and formalize a new anomaly detection task in multi-variate time series: intrinsic anomaly detection (Sec. 2). Second, we present a method to tackle intrinsic anomaly detection (Sec. 3) which satisfies the afore-mentioned desiderata. In particular, we propose a novel adaptation of unsupervised time series representations (Franceschi et al., 2019) yielding environment-invariant embeddings. Third, we provide an initial set of diverse data sets that allows to study this novel problem in a meaningful way: wind turbines as an IoT use case, a semi-synthetic DevOps data set, a swinging pendulum simulation, and a fully synthetic data set based on simple generative models. Our experiments in Sec. 4 show that our approach based on environment-invariant embeddings performs favorably when compared against standard anomaly detection methods as well as natural baselines.

2 Intrinsic Anomaly Detection: Problem Statement

Let $\mathbf{z} \in \mathbb{R}^{D \times T}$ be a multi-variate, equally spaced time series of length T with D dimensions corresponding to a system/environment combination. We denote by $\mathbf{z}_{t:t+j} = (\mathbf{z}_t, \mathbf{z}_{t+1}, \dots, \mathbf{z}_{t+j})$ a time series snippet of \mathbf{z} . The standard way to define an anomaly at time t for a multi-variate time series is to say that at time t we have an anomaly if \mathbf{z}_t differs from its expected value, denoted by $\hat{\mathbf{z}}_t$, by more than a threshold τ (Blázquez-García et al., 2021). A canonical choice in anomaly detection for multi-variate time series is a predictive time series model that, given the history of the multi-variate time series, provides an estimate $\hat{\mathbf{z}}_t$ via a forecast or a probabilistic generative model.

In the context of this paper, we have additional structure that we can take advantage of by assuming a decomposition $\mathbf{z} = (\mathbf{x}, \mathbf{y})$ such that time series $\mathbf{x} \in \mathbb{R}^{N \times T}$ allows to predict time series $\mathbf{y} \in \mathbb{R}^{M \times T}$, $D = N + M$, via a function h (modulo an error term ε):

$$\mathbf{y}_t = h(\mathbf{x}_{0:t}; \mathbf{y}_{0:t-1}) + \varepsilon. \quad (1)$$

For all t we have the residual $\delta_t = d(\mathbf{y}_t, h(\mathbf{x}_{0:t}; \mathbf{y}_{0:t-1}))$ for a distance metric d . We call \mathbf{x} the set of *environmental* and \mathbf{y} the set of *system* time series.

We define an *extrinsic anomaly* at time t as an anomaly solely in \mathbf{x} , i.e., at time t we have $d(\mathbf{x}_t, \hat{\mathbf{x}}_t) > \tau_x$ for a threshold τ_x . At the same time, the functional dependency between \mathbf{x} and \mathbf{y} remains unchanged, meaning that the residual signal δ_t does not exhibit an anomaly: $\delta_t \leq \tau_y$. Conversely, an *intrinsic anomaly* at time t consists of an anomaly in the residual signal δ_t itself, i.e., for a threshold τ_y we have $d(\mathbf{y}_t, \hat{\mathbf{y}}_t) = d(\mathbf{y}_t, h(\mathbf{x}_{0:t}; \mathbf{y}_{0:t-1})) > \tau_y$.

We have not further prescribed what h is apart from being a multi-variate function; h may be a highly non-linear and/or stochastic function that depends on the state of the system as well as (lagged) environmental variables. Depending on the application scenario, h is either given or needs to be obtained. For example, we may have a known physical model describing a system’s interaction with the environment or we may assume the need to learn a complex function $h_V \approx h$ from data. In the former case, this relationship between environment and system state will hold also for extreme values in the environment (an extrinsic anomaly), but break whenever the system exhibits internal faults. In the latter case, we may be able to reliably learn parameters V for h_V assuming that intrinsic anomalies are rare. In the data sets that we consider, it is a realistic assumptions that we must learn h_V , so we focus on this scenario.

3 Representation Learning for Intrinsic Anomaly Detection

In designing methods for intrinsic anomaly detection, we recall desiderata from the introduction: they must be able to separate intrinsic from extrinsic anomalies, rely on unsupervised learning, and allow to identify similar time series effectively in data quality improvement tasks. We assume that the decomposition into environmental and system time series is given (and does not need to be identified), however we do not assume the functional dependence h to be known.

Our approach relies on two main ingredients: (i) learning effective representations via contrastive learning; and (ii) equipping them to distinguish intrinsic and extrinsic anomalies by forcing representations to be

invariant to the environment. We motivate both ingredients separately in Sec. 3.1 and 3.2 respectively and then present the proposed models.

3.1 Contrastive Losses and Anomaly Detection

Time series representation learning techniques such as (Franceschi et al., 2019) aim to provide general-purpose representations that are independent of the downstream task. However, there is a particularly close connection to popular approaches in anomaly detection. For example, Ruff et al. (2018) propose to learn representations of data points whose enclosing hyper-sphere has minimal size, formally

$$\min_W \sum_i (f_W(\mathbf{z}_{i:i+\ell}) - \mathbf{c})^2 + \Omega. \quad (2)$$

Here, $\mathbf{z}_{i:i+\ell}$ are contiguous time series snippets of length ℓ of \mathbf{z} , f_W is an embedding function $R^{D \times \ell} \rightarrow R^d$ parameterized by W , $\mathbf{c} \in R^d$ is a given center of a hyper-sphere, and Ω is a regularization term. Ruff et al. (2018) argue that under the common and realistic assumption that anomalies are rare, a reasonable embedding function f_W would be learnt such that embeddings of normal time series are close to the cluster center \mathbf{c} while abnormal ones have a larger distance to \mathbf{c} . The distance between $f_W(\mathbf{z}_{i:i+\ell})$ and \mathbf{c} can hence be treated as a metric for the normality of a time series in the embedded space.

The connection to contrastive learning is then intuitively clear as they construct embeddings equipped with a distance function that fulfills a similar purpose. Instead of choosing a cluster center explicitly,¹ typical contrastive losses flexibly choose points that are (heuristically) close to each other (e.g., close in time for time series). We formalize this as

$$\min_W \sum_i \sum_j d(f_W(\mathbf{z}_{i:i+\ell}), f_W(\mathbf{z}_{j:j+k})) + \Omega, \quad (3)$$

where d is a distance function in the embedding space (e.g., ℓ_2 as in (2)). Typically, the cluster centers $\mathbf{z}_{j:j+k}$ are referred to as *reference* examples and $\mathbf{z}_{i:i+\ell}$ are *positive* examples with i, ℓ randomly chosen such that $\mathbf{z}_{i:i+\ell} \subseteq \mathbf{z}_{j:j+k}$.

In order to guarantee the second property of (2) – that abnormal points are far from each other – many contrastive losses explicitly require that points that are (heuristically) different are further away in the embedding space. These *negative* examples should be far apart in terms of the cluster centers, leading to the desired property that individual hyper-spheres have small volume (normal values are concentrated) and hyper-spheres among themselves are subject to a repelling effect (summarized by Ω in (3)).

3.2 Representations for Intrinsic Anomaly Detection

While contrastive losses allow for standard anomaly detection in multi-variate time series (see e.g., Blázquez-García et al. (2021) for an overview), they do not allow fine-grained distinctions into intrinsic and extrinsic anomalies. Following the arguments above, we expect extrinsic and intrinsic anomalies to correspond to outliers in the embedding space because they are rare. It is unclear however why an embedding of an extrinsic anomaly, should necessarily be distant from an embedding of an intrinsic anomaly. To guarantee that we can separate extrinsic and intrinsic anomalies in the embedding space, it is natural to consider the inclusion of an inductive bias, namely an invariance of the representations towards the environment, to ensure this separation. First, note that embeddings that are invariant to changes in the environment do not carry information about the environment, analogous to the ideal residual signal in Sec. 2. For an environment-invariant embedding, intrinsic normality corresponds to proximity in the embedding space (because this is the frequent case), while intrinsic anomalies violate the standard invariance and would hence be more distant in the embedding space. Second, we can modify contrastive losses explicitly to encode that a broken functional relationship between environment and system variables correspond to greater distance in the embedding space.

¹Ruff et al. (2018) use the average of the initially found embeddings of the training set vectors in the first iteration of the optimization algorithm as cluster centers.

Adversarial learning for Environment-Invariance For obtaining representations of \mathbf{z} that are invariant to the environment \mathbf{x} , a popular choice is to apply an adversarial learning approach [Xie et al. \(2018\)](#); [Long et al. \(2017\)](#) which we adapt to our unsupervised setting. We train the predictor g_U in an adversarial manner jointly with the embedding model: The predictor’s parameters are trained to maximize the likelihood of \mathbf{x} given embeddings $f_W(\mathbf{z})$; the weights of the embedding model f_W are trained to maximize the error of the predictor. This encourages the embeddings to become invariant to \mathbf{x} . Note that for the prediction task, we use a multi-class classification approach by discretizing \mathbf{x} appropriately. Hence, we compute the negative log probability of the correct class as our loss, i.e.,

$$\mathcal{L}_{\text{adv}}(g_U(f_W(\mathbf{z}_{i:j})), \mathbf{x}_{i:j}) = -\log \frac{1}{g_U(f_W(\mathbf{z}_{i:j}))_{\mathbf{x}_{i:j}}}. \quad (4)$$

For g_U we use a neural network with a softmax function as the final layer. The full loss is given by

$$\mathcal{L}_{\text{adv}}(W, U) = \sum_{i,j} \mathcal{L}_{\text{adv}}(g_U(f_W(\mathbf{z}_{i:j})), \mathbf{x}_{i:j}). \quad (5)$$

Negative Examples in Contrastive Losses For embeddings of \mathbf{z} , we can equip (3) with negative examples that explicitly encode when the dependency structure is broken. We construct these negative examples as system and environment variables originating from different time snippets. We denote $\mathbf{z}^{\text{pos}} = (\mathbf{x}^{\text{pos}}, \mathbf{y}^{\text{pos}}) = (\mathbf{x}_{i:i+\ell}, \mathbf{y}_{i:i+\ell})$ as a positive and $\mathbf{z}^{\text{ctx}} = (\mathbf{x}^{\text{ctx}}, \mathbf{y}^{\text{ctx}}) = (\mathbf{x}_{j:j+k}, \mathbf{y}_{j:j+k})$ as a reference time series snippet where i, j, k, ℓ are chosen (randomly) such that positive examples are contained in the reference time series. In the construction of negative examples, we explicitly break the dependency structure between \mathbf{x} and \mathbf{y} in defining $\mathbf{z}^{\text{neg}} = (\mathbf{x}^{\text{neg}}, \mathbf{y}^{\text{pos}}) = (\mathbf{x}_{r:r+\ell}, \mathbf{y}_{i:i+\ell})$ where r is (randomly) chosen such that $\mathbf{x}_{\text{neg}} \cap \mathbf{x}_{\text{pos}} \approx \emptyset$. Figure 2a provides an illustration. The contrastive loss uses these three sample types such that time series with default dependence structure should be embedded close to each other while time series with varying dependence structures should be distant from each other. For an embedding network f_W with parameters W , the loss function takes the following form:

$$\mathcal{L}_{\text{contr}}(W) = \sum_{\text{pos}} \sum_{\text{ctx}} d(f_W(\mathbf{z}^{\text{pos}}), f_W(\mathbf{z}^{\text{ctx}})) - \sum_{\text{neg}} \sum_{\text{ctx}} d(f_W(\mathbf{z}^{\text{neg}}), f_W(\mathbf{z}^{\text{ctx}})). \quad (6)$$

We aim to minimize (6). Note that (6) is amenable to batch optimization and we can further construct negative examples such that negative environment variables are chosen from a different series in the batch.

3.3 Model Overview

Our approach consists of two main components: a *predictor network* g_U for environment invariance, and an *embedding network* f_W which learns embeddings using contrastive losses. Figure 2b depicts the main components of our approach. For g_U , we choose a single-layer feed-forward neural network to place more onus on f_W to become invariant to the environment. For discretization of \mathbf{x} , we choose standard quantile-based binning with 20 buckets.

The basic building block of our embedding network architecture consists of stacked temporal dilated causal convolutions ([Bai et al., 2018](#)) following ([Franceschi et al., 2019](#)). We choose such a temporal convolutional neural network (TCN) for its speed of computation and its general robustness to facilitate experimentation.

The final loss is a combination of a contrastive loss with a regularizer to obtain environment invariance, which is summarized as follows:

$$\mathcal{L}(W, U) = \mathcal{L}_{\text{contr}}(W) - \lambda \mathcal{L}_{\text{adv}}(W, U), \quad (7)$$

where $\mathcal{L}_{\text{contr}}(W)$ is the contrastive loss (6), $\mathcal{L}_{\text{adv}}(W, U)$ is the environment-invariance loss (5), and λ is a hyperparameter that governs the trade-off between them. We seek a saddle point (\hat{W}, \hat{U}) such that $\hat{W} = \arg \min_W \mathcal{L}(W, \hat{U})$ and $\hat{U} = \arg \min_U \mathcal{L}(\hat{W}, U)$. We use a gradient-reversal layer between f and g to identify the saddle point in (7) as proposed in ([Ganin et al., 2016](#)). [Moyer et al. \(2018\)](#) provide further theoretical and practical justifications for it.

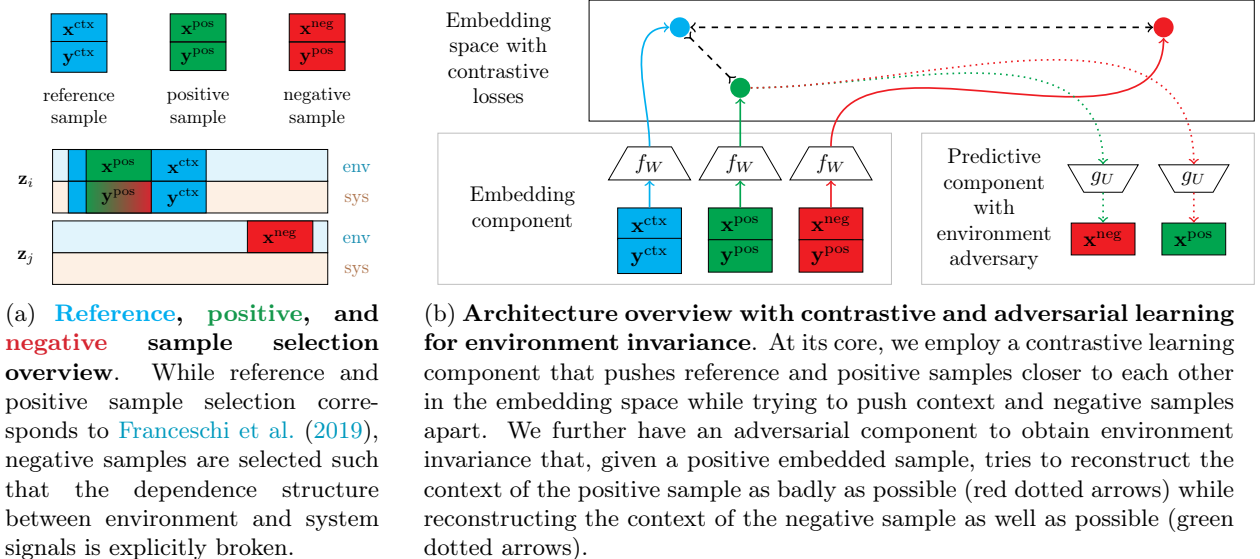


Figure 2: Overview of the sample selection process for contrastive learning and architecture diagram.

Table 1: Data set summary statistics. Each dataset consists of multiple distinct sub-systems. For each system, we have a number of time series snippets available with length T . N and M denote the number of environmental and system variables, respectively.

Dataset	# Systems	# Series	T	N	M
Synthetic	1 system	360	1440	2	2
Pendulum	1 pendulum	300	144	1	2
Turbine	4 turbines	360	144	5	4
DevOps	1 app	128	128	1	3

4 Experiments

In our experiments, we empirically evaluate our approach both quantitatively and qualitatively. Public time series data sets for (standard) anomaly detection² are not suitable for intrinsic anomaly detection, so we do not consider them. Instead, we evaluate on four different data sets, each of which allows for a separation into environmental and system signals. We discuss these data sets first, then describe our evaluation approach and the models under consideration, and finally present our results.

4.1 Datasets

The selection of benchmark datasets aims to balance physical and virtual systems as well as synthetic and real-world data. Note that synthetic data exhibits perfect labels, while real-world data typically does not. While unfortunate, we believe that this subjectivity and noisiness must be embraced as fundamental in the task. Hence, we place additional emphasis on qualitative experiments. Appendix A contains further details and illustrations on the data sets and Table 1 captures details of the datasets under consideration.

Synthetic We generate a synthetic dataset based on a simple sinusoidal generative model. We generate two environmental signals, as well as two system signals. We inject two types of anomalies into the data: (i) extrinsic anomalies, i.e., anomalies in the environmental which are also instantly reflected in the system variables and (ii) intrinsic anomalies only in the system variables.

²Wu and Keogh (2021) convincingly argue that many of these datasets should be abandoned.

Pendulum We consider the case of a swinging pendulum with added control signals, where we control the dampening of the acceleration from the outside as an environmental signal (towards which we want to be invariant). As intrinsic anomalies, we consider those where we inject an anomaly as a change in the length of the chord, which we capture as part of the system signal. Our aim with this data set is to understand how well our models handle cases where the dependency structure between system and environment is significantly more complex (i.e. time-shifted and non-linear) than in the Synthetic data set.

DevOps is a new, semi-synthetic data set³ which resembles data sets behind corporate firewalls. It is based on a cloud-based microservice demo app,⁴ commonly used in a DevOps context (Wu et al., 2020). The environment for the application are user interactions with the app, approximated by the network outbound traffic of an auxiliary application that induces synthetic load/user behaviour on the app. The system signals consist of metrics such as CPU consumption, memory or disk consumption of the app. We inject anomalies both in the user behavior which lead to extrinsic anomalies and in the internal state to obtain intrinsic anomalies. Note that although we have almost total control of the application, the labelling of anomalies is still imperfect, thereby adding further to the complications of public anomaly detection benchmarks (Wu and Keogh, 2021).

Wind Turbine is a public wind turbine data set by Energias de Portugal.⁵ The time series panel can be separated into environmental signals (e.g., wind speed/direction, ambient temperature) and system signals (e.g., rotational speeds of generators, temperature on different components, power output). Note that this data set contains only few (43) labelled anomalies and visual inspections of the data reveals inconsistencies with these labels, see e.g., Figure 3c. Hence, purely quantitative evaluations cannot be taken at face value. Operating under this limitation, we illustrate the versatility of our approach qualitatively in Sec. 4.4.

4.2 Model and Evaluation Details

For a comprehensive empirical comparison, we consider the following families of approaches: (i) approaches based on deep embeddings to varying degree of complexity, the most closely related to our approach; (ii) approaches based on classical time series embeddings; and (iii) standard anomaly detection methods on time series. We consider these approaches on both the original time series and on the residual signal. We further note that we only perform hyperparameter tuning on the Synthetic data set as we do not have enough labels available on other datasets. Appendix B provides more fine-grained details on particular hyperparameter choices for the models described next.

Deep Embeddings We consider the following models in our comparison which we list in increasing order of complexity. We can choose to ignore the functional dependency h and learn representations of \mathbf{z} with a TCN equipped with contrastive losses. We denote this approach as **BasicEmb**. Next, we propose a two-step approach for environment-invariance by explicitly approximating the functional dependence h between \mathbf{x}_t and \mathbf{y}_t using a neural network h_V first, and then learning embeddings of the *residual* signal $\hat{\delta} := h_V(\mathbf{x}) - \mathbf{y}$ in a second step. We refer to this approach as **ResEmbRegr**. Finally, we use the approach outlined in Sec. 3 which we call **EnvInvEmb**. We choose $\lambda = 10^{-3}$ as determined by an ablation study (see Appendix B).

Classical Embeddings We compare against two instances of (Lubba et al., 2019): **Catch22** and **ResCatch22** which compute a feature vector per original and residual time series respectively similar to **ResEmbRegr**.

Anomaly Detection Methods We consider a simple thresholding mechanism, **ResTresh**, which thresholds the residual signal $\hat{\delta}$ that is also obtained in **ResEmbRegr**; **OmniAnomaly** (Su et al., 2019a) as a popular example for deep anomaly detection; and as examples for classical approaches: Isolation Forests (Liu et al., 2008) IF, Local Outlier Factor (Breunig et al., 2000) LOF, and One-class SVM (Schölkopf et al., 1999) OCSVM.

³We will open-source both the raw data as well as the set-up to produce the data.

⁴<https://github.com/microservices-demo/microservices-demo>

⁵<https://opendata.edp.com/pages/homepage/>

Table 2: AUROC results on the intrinsic anomaly detection task.

Category	Signal Type	Detection Approach	Synthetic	Pendulum	DevOps	Turbine
Deep Embeddings	Original	EnvInvEmb	0.999 (± 0.002)	0.980 (± 0.002)	0.587 (± 0.007)	0.756 (± 0.022)
		BasicEmb	0.512 (± 0.022)	0.969 (± 0.013)	0.535 (± 0.041)	0.632 (± 0.015)
	Residual	ResEmbRegr	1.000 (± 0.000)	0.951 (± 0.015)	0.532 (± 0.036)	0.725 (± 0.018)
Classic Embeddings	Original	Catch22	0.494 (± 0.008)	0.904 (± 0.000)	0.573 (± 0.000)	0.512 (± 0.000)
	Residual	ResCatch22	1.000 (± 0.000)	0.891 (± 0.000)	0.577 (± 0.000)	0.680 (± 0.000)
Anomaly Detection	Original	LOF	0.557 (± 0.016)	0.541 (± 0.042)	0.518 (± 0.033)	0.578 (± 0.026)
		IF	0.500 (± 0.014)	0.502 (± 0.024)	0.489 (± 0.013)	0.512 (± 0.018)
		OCSVM	0.499 (± 0.022)	0.500 (± 0.013)	0.569 (± 0.025)	0.521 (± 0.017)
		OmniAnomaly	0.788 (± 0.108)	0.642 (± 0.082)	0.513 (± 0.023)	0.561 (± 0.026)
	Residual	LOF	0.537 (± 0.046)	0.467 (± 0.030)	0.573 (± 0.070)	0.679 (± 0.045)
		IF	0.513 (± 0.020)	0.525 (± 0.015)	0.507 (± 0.008)	0.534 (± 0.012)
		OCSVM	0.546 (± 0.012)	0.534 (± 0.009)	0.571 (± 0.013)	0.533 (± 0.010)
		OmniAnomaly	0.801 (± 0.075)	0.717 (± 0.113)	0.435 (± 0.028)	0.492 (± 0.067)
		ResTresh	1.000 (± 0.011)	0.510 (± 0.000)	0.619 (± 0.000)	0.845 (± 0.032)

Table 3: The ℓ_2 distance gap between embeddings of correct and incorrect classes on the anomaly detection task. Environment-invariant embeddings induce the largest gap.

	BasicEmb	ResEmbRegr	Catch22	EnvInvEmb
Synthetic	0.051 (± 0.041)	0.641 (± 0.314)	0.008 (± 0.01)	1.944 (± 0.039)
Pendulum	0.446 (± 0.059)	0.433 (± 0.074)	0.019 (± 0.00)	0.486 (± 0.178)
DevOps	0.014 (± 0.006)	0.035 (± 0.008)	0.013 (± 0.00)	0.042 (± 0.007)
Turbine	0.075 (± 0.007)	0.319 (± 0.103)	0.004 (± 0.00)	0.450 (± 0.085)

Table 4: F-1 scores for the anomaly type classification task. While primarily designed to capture intrinsic anomalies, the disentanglement yielded by environment-invariant embeddings allows for the identification of extrinsic anomalies.

	BasicEmb	ResEmbRegr	Catch22	ResCatch22	EnvInvEmb
2-class	0.85 (± 0.04)	0.98 (± 0.01)	0.85 (± 0.02)	0.99 (± 0.01)	0.99 (± 0.01)
3-class	0.74 (± 0.03)	0.59 (± 0.08)	0.71 (± 0.03)	0.64 (± 0.06)	0.89 (± 0.03)

Evaluation Details For each dataset, we break the original multi-variate time series into time series snippets (length described in Table 1) and classify each snippet as abnormal if it contains an intrinsic anomaly. Although the length of an intrinsic anomaly is variable, intrinsic anomalies appear as intervals in our data sets and not as isolated single-point anomalies. While embedding-based approaches can handle variable-length input series, classic embeddings and traditional anomaly detection approaches provide an anomaly score for each time step. To compare these methods on an equal footing, we aggregate anomaly scores from individual time steps to a single score for a full snippet. We report mean results over 5 random seeds.

4.3 Quantitative Results

We study both the raw intrinsic anomaly detection performance as well as the disentanglement of extrinsic and intrinsic anomalies in the learned latent spaces.

Intrinsic Anomaly Detection Performance Acknowledging recent concern on the validity of time series anomaly benchmarks (Kim et al., 2021), our main quantitative results report AUROC scores on the intrinsic anomaly detection task. For the **ResTresh** method, we compute the AUROC score based on the maximum residual value over the full residual series. For the embedding-based approaches, we use a k -nearest-neighbor classifier ($k = 5$) in the embedding space to determine a discrete anomaly label.

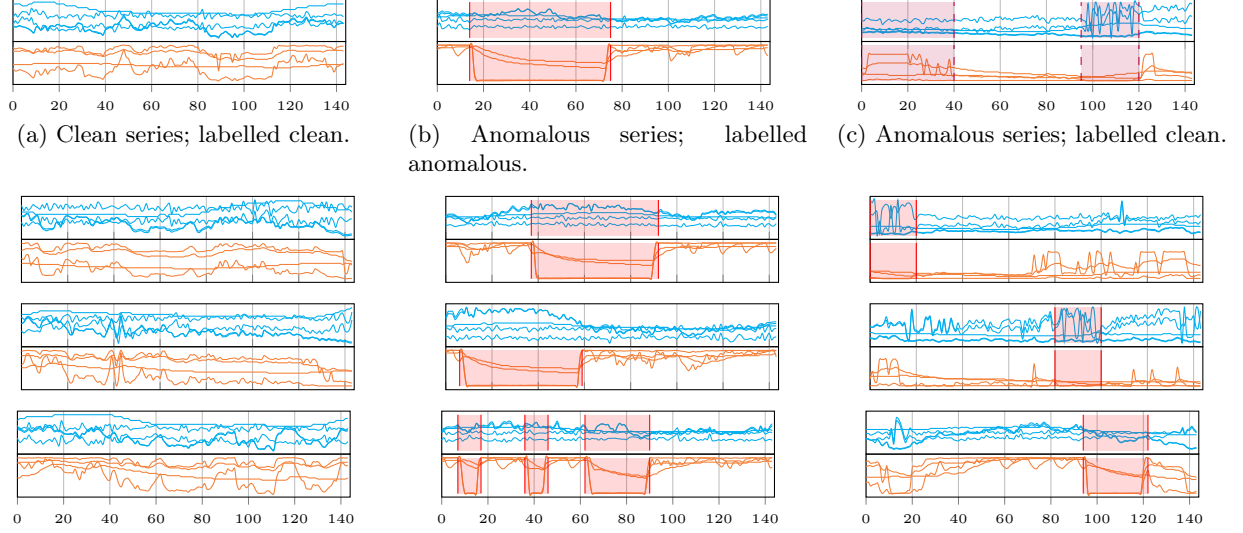


Figure 3: Nearest-neighbor analysis of **EnvInvEmb** on the Turbine dataset. Each panel shows environmental signals on the top (blue signals) and system signals at the bottom (orange signals). The first row shows (a) a normal reference series; (b) an abnormal reference series (anomaly between time steps 20 and 70); and (c) an anomalous reference series that was mistakenly labeled as clean in the test set. Below each of these series we show 3 nearest neighbors in the learned embedding space. For the left and center column, both the correct label and our predicted label match. For series (c), the reference time series is labelled as clean, but its nearest neighbors are abnormal.

Table 2 summarizes our main quantitative results. First, we note that the difficulty of intrinsic anomaly detection differs widely with the data sets. For example, intrinsic anomaly detection seems relatively easier on the Turbine data set compared with the DevOps data set despite the latter being semi-synthetically generated with controlled labels. Second, we note that **EnvInvEmb** leads to overall superior results when comparing the embedding based approaches (the first three rows in Table 2) and is overall competitive results in many cases, but not always. For the DevOps and Turbine data sets, **ResTresh** is overall best by a margin. The explanation here is that the simple instantaneous mapping of **ResTresh** is a good inductive bias for these data sets – however, this is in particular not the case for Pendulum. For the Pendulum data set, it is worthwhile to note that **EnvInvEmb** delivers an overall superior approach despite the complex non-linear interaction between the environmental and system signals and only a linear environment-predictor component. We further note that our approach is superior to the other anomaly detection methods consistently and independently whether we apply the anomaly detection methods directly on the time series or when taking the residual.

Embedding Space Distances For methods that produce a mapping onto an embedding space, we can further determine whether any particular (embedded) time series is closer to the mean embedding of the respective correct/incorrect class. Concretely, we can compute the gap between the distance to the correct class for the respective series and the distance to the incorrect class and average this quantity over all series in the test set. Results are presented in Table 3. This complements the AUROC results in Table 2 by providing an indication of the degree of entanglement in the embedding space and the resulting nearest-neighborhood structure. Overall, we observe that environment-invariant embeddings produce the largest gap.

Identifiability of Extrinsic vs Intrinsic Anomalies We further provide results on the identifiability of both extrinsic anomalies and intrinsic anomalies. For the Synthetic dataset, we create two distinct labelings: (i) A *2-class* labeling where both normal series snippets and extrinsic-anomalous series are assigned the label 0 and intrinsic anomalies only are assigned the label 1; and (ii) a *3-class* labeling where normal snippets are labeled as 0, extrinsic anomalies are labeled as 1, and intrinsic anomalies are labeled as 2. Performance on the first labeling indicates how well each method is capable of separating intrinsic anomalies from all

encounterable scenarios (1-vs-all setting) while performance on the second labeling indicates the level of disentanglement of individual anomaly types in the embedding space. Note that our evaluation in Table 2 relies on 2-class labeling.

We report the weighted F-1 scores for both labeling strategies as part of Table 4. We observe that environment-invariant embeddings provide both (i) strong 1-vs-all performance (2-class) and at the same time still (ii) enable superior identification of normal and extrinsic-anomalous series (3-class). We also find that residual-based approaches (i.e. `ResEmbRegr` and `ResCatch22`) provide strong 1-vs-all performance but they do so at the expense of extrinsic anomaly identification. These findings suggests that environment-invariant embeddings enable us to learn more complex non-linear dependence structures and patterns that go beyond simple residual signals.

4.4 Qualitative Results: A Case Study On Turbines

The embeddings induce a nearest-neighbor structure which allows us to navigate the time series corpus via distances. This can be helpful in exploring the data set and uncovering data or label issues. In Figure 3, we show this in qualitative results for environment-invariant embeddings on the Turbine dataset. The first two columns show sanity checks: reference time series (top row) labelled as normal or abnormal have as their nearest neighbors (same column as the reference time series) normal and abnormal time series, respectively. Despite the multi-variate nature of the data, visual inspection confirms the plausibility of the nearest neighbors. The last column in Figure 3 shows an example where a reference time series is labelled as normal, but its nearest neighbors consist of time series that are labeled as abnormal. This could point to a labelling issue, i.e., it may make sense to re-label the reference time series in column (c) as abnormal for the abnormal stretches 0-40 and 100-130.

5 Related work

Anomaly detection in time series has a rich body of literature, see e.g., [Su et al. \(2019a\)](#); [Carmona et al. \(2021\)](#); [Ren et al. \(2019\)](#); [Ayed et al. \(2020\)](#); [Wu and Keogh \(2021\)](#); [Su et al. \(2019b\)](#); [Guha et al. \(2016\)](#); [Blázquez-García et al. \(2021\)](#) for a recent overview. While different variants of anomalies are the subject of discussion, we are not aware of a prior discussion of intrinsic anomalies (see e.g., [Foorthuis \(2021\)](#) for a comprehensive overview of anomaly types). Intrinsic anomaly detection is a subset of the more general class of contextual anomalies where *context* is more broadly and fuzzily defined ([Han et al., 2012](#)). The closest relative are conditional anomalies ([Song et al., 2007](#)) defined for tabular data, however they ignore the interplay between extrinsic and intrinsic anomalies. We are not aware of other publicly available multi-variate time series data sets that lend themselves to targeted study of intrinsic anomaly detection. Existing detection methods can be adopted to the intrinsic anomaly detection problem by relying on the residual signal, however our experiments show that custom-built methods are superior. A possibility for future work is the refinement of our problem statement with a causal treatment, see [Janzing et al. \(2019\)](#) for an example outside the time series context as well as discovery of the causal dependency structure ([Haufe et al., 2009](#); [Qiu et al., 2020, 2012](#)).

Similar to anomaly detection for time series, representation learning for time series has a rich body of literature, e.g., [Franceschi et al. \(2019\)](#); [Zerveas et al. \(2021\)](#); [Lubba et al. \(2019\)](#); [Christ et al. \(2017\)](#). The connection between anomaly detection and contrastive losses is not new (see e.g., [Tack et al. \(2020\)](#); [Sohn et al. \(2021\)](#) for recent examples), but it is under-explored in the time series domain. While we extend [Franceschi et al. \(2019\)](#) for practical reasons such as speed of experimentation and general robustness, we remark our approach carries over also to other architectures, such as [Zerveas et al. \(2021\)](#).

Arguably, representation learning is less prominently discussed in time series compared to other disciplines such as computer vision or natural language processing ([Chen et al., 2020](#); [van den Oord et al., 2019](#); [He et al., 2020](#); [Fang et al., 2020](#); [Jaiswal et al., 2021](#)). While these fields consider learning invariant representations a central question, see e.g., [Ganin et al. \(2016\)](#); [Moyer et al. \(2018\)](#); [Akash et al. \(2021\)](#); [Achille and Soatto \(2018\)](#), this has not been the case for the time series domain to the best of our knowledge. Correspondingly, work on domain adaptation is in its infancy ([Jin et al., 2021](#)). Our approach attempts to change this and relies heavily on [Xie et al. \(2018\)](#) by considering invariance with respect to variables included in the data.

6 Conclusion

We present a novel variation of the anomaly detection task in multi-variate time series where an intrinsic anomaly manifests itself as a departure from the typical functional relationship between an environment and a system. Our main method for addressing intrinsic anomaly detection relies on unsupervised time series representation learning. We combine contrastive losses for representation learning with an adversarial learning component that yields environment-invariant embeddings. This environment invariance allows to isolate intrinsic anomalies in the embedding space and leads to favorable performance in the detection tasks. Our empirical evaluation establishes both a framework for evaluating intrinsic anomalies and introduces purposefully designed data sets. We show that the resulting representations allow for meaningful data interactions by exploring nearest neighbors in the embedding space, thereby addressing data quality issues ubiquitous in anomaly detection datasets.

References

- Alessandro Achille and Stefano Soatto. Emergence of invariance and disentanglement in deep representations. *Journal of Machine Learning Research*, 19(50):1–34, 2018. URL <http://jmlr.org/papers/v19/17-646.html>.
- Aditya Kumar Akash, Vishnu Suresh Lokhande, Sathya N. Ravi, and Vikas Singh. Learning invariant representations using inverse contrastive loss, 2021.
- Fadhel Ayed, Lorenzo Stella, Tim Januschowski, and Jan Gasthaus. Anomaly detection at scale: The case for deep distributional time series models, 2020.
- Shaojie Bai, J. Zico Kolter, and Vladlen Koltun. An empirical evaluation of generic convolutional and recurrent networks for sequence modeling, 2018.
- Ane Blázquez-García, Angel Conde, Usue Mori, and Jose A. Lozano. A review on outlier/anomaly detection in time series data. *ACM Comput. Surv.*, 54(3), apr 2021. ISSN 0360-0300. doi: 10.1145/3444690. URL <https://doi.org/10.1145/3444690>.
- Jasmin Bogatinovski, Sasho Nedelkoski, Alexander Acker, Florian Schmidt, Thorsten Wittkopp, Soeren Becker, Jorge Cardoso, and Odej Kao. Artificial intelligence for it operations (aiops) workshop white paper, 2021.
- Markus M Breunig, Hans-Peter Kriegel, Raymond T Ng, and Jörg Sander. Lof: identifying density-based local outliers. In *Proceedings of the 2000 ACM SIGMOD international conference on Management of data*, pages 93–104, 2000.
- Chris U. Carmona, François-Xavier Aubet, Valentin Flunkert, and Jan Gasthaus. Neural contextual anomaly detection for time series, 2021.
- Ting Chen, Simon Kornblith, Mohammad Norouzi, and Geoffrey Hinton. A simple framework for contrastive learning of visual representations. In *International conference on machine learning*, pages 1597–1607. PMLR, 2020.
- Maximilian Christ, Andreas W. Kempa-Liehr, and Michael Feindt. Distributed and parallel time series feature extraction for industrial big data applications, 2017.
- Hongchao Fang, Sicheng Wang, Meng Zhou, Jiayuan Ding, and Pengtao Xie. Cert: Contrastive self-supervised learning for language understanding, 2020.
- Ralph Foorthuis. On the nature and types of anomalies: a review of deviations in data. *International Journal of Data Science and Analytics*, 12(4):297–331, Aug 2021. ISSN 2364-4168. doi: 10.1007/s41060-021-00265-1. URL <http://dx.doi.org/10.1007/s41060-021-00265-1>.
- Jean-Yves Franceschi, Aymeric Dieuleveut, and Martin Jaggi. Unsupervised scalable representation learning for multivariate time series. *arXiv preprint arXiv:1901.10738*, 2019.
- Yaroslav Ganin, Evgeniya Ustinova, Hana Ajakan, Pascal Germain, Hugo Larochelle, François Laviolette, Mario Marchand, and Victor Lempitsky. Domain-adversarial training of neural networks. *The journal of machine learning research*, 17(1):2096–2030, 2016.
- Sudipto Guha, Nina Mishra, Gourav Roy, and Okke Schrijvers. Robust random cut forest based anomaly detection on streams. In *Proceedings of the 33rd International Conference on International Conference on Machine Learning - Volume 48*, ICML’16, page 2712–2721. JMLR.org, 2016.
- Jiawei Han, Micheline Kamber, and Jian Pei. Data mining concepts and techniques, third edition, 2012. URL http://www.amazon.de/Data-Mining-Concepts-Techniques-Management/dp/0123814790/ref=tmm_hrd_title_0?ie=UTF8&qid=1366039033&sr=1-1.
- Stefan Haufe, Guido Nolte, Klaus-Robert Mueller, and Nicole Kraemer. Sparse causal discovery in multivariate time series, 2009.
- Kaiming He, Haoqi Fan, Yuxin Wu, Saining Xie, and Ross Girshick. Momentum contrast for unsupervised visual representation learning, 2020.

- Ashish Jaiswal, Ashwin Ramesh Babu, Mohammad Zaki Zadeh, Debapriya Banerjee, and Fillia Makedon. A survey on contrastive self-supervised learning, 2021.
- Dominik Janzing, Kailash Budhathoki, Lenon Minorics, and Patrick Blöbaum. Causal structure based root cause analysis of outliers, 2019.
- Xiaoyong Jin, Youngsuk Park, Danielle C. Maddix, Yuyang Wang, and Xifeng Yan. Domain adaptation for time series forecasting via attention sharing, 2021.
- Siwon Kim, Kukjin Choi, Hyun-Soo Choi, Byunghan Lee, and Sungroh Yoon. Towards a rigorous evaluation of time-series anomaly detection. *arXiv preprint arXiv:2109.05257*, 2021.
- Christian Krupitzer, Tim Wagenhals, Marwin Züfle, Veronika Lesch, Dominik Schäfer, Amin Mozaffarin, Janick Edinger, Christian Becker, and Samuel Kounnev. A survey on predictive maintenance for industry 4.0. *arXiv preprint arXiv:2002.08224*, 2020.
- Richard Kurle, Syama Sundar Rangapuram, Emmanuel de Bézenac, Stephan Günnemann, and Jan Gasthaus. Deep rao-blackwellised particle filters for time series forecasting. *Advances in Neural Information Processing Systems*, 33, 2020.
- Yangguang Li, Zhen Ming (Jack) Jiang, Heng Li, Ahmed E. Hassan, Cheng He, Ruirui Huang, Zhengda Zeng, Mian Wang, and Pinan Chen. Predicting node failures in an ultra-large-scale cloud computing platform: An aiops solution. *ACM Trans. Softw. Eng. Methodol.*, 29(2), April 2020. ISSN 1049-331X. doi: 10.1145/3385187. URL <https://doi.org/10.1145/3385187>.
- Fei Tony Liu, Kai Ming Ting, and Zhi-Hua Zhou. Isolation forest. In *2008 eighth ieee international conference on data mining*, pages 413–422. IEEE, 2008.
- Björn Lohrmann and Odej Kao. Processing smart meter data streams in the cloud. In *2011 2nd IEEE PES International Conference and Exhibition on Innovative Smart Grid Technologies*, pages 1–8, 2011. doi: 10.1109/ISGTEurope.2011.6162747.
- Mingsheng Long, Zhangjie Cao, Jianmin Wang, and Michael I Jordan. Conditional adversarial domain adaptation. *arXiv preprint arXiv:1705.10667*, 2017.
- Bin Lu, Yaoyu Li, Xin Wu, and Zhongzhou Yang. A review of recent advances in wind turbine condition monitoring and fault diagnosis. In *2009 IEEE Power Electronics and Machines in Wind Applications*, pages 1–7, 2009. doi: 10.1109/PEMWA.2009.5208325.
- Carl H Lubba, Sarab S Sethi, Philip Knaute, Simon R Schultz, Ben D Fulcher, and Nick S Jones. catch22: Canonical time-series characteristics. *Data Mining and Knowledge Discovery*, 33(6):1821–1852, 2019.
- Daniel Moyer, Shuyang Gao, Rob Brekelmans, Greg Ver Steeg, and Aram Galstyan. Invariant representations without adversarial training. In *Proceedings of the 32nd International Conference on Neural Information Processing Systems, NIPS’18*, page 9102–9111, Red Hook, NY, USA, 2018. Curran Associates Inc.
- Sasho Nedelkoski, Jorge Cardoso, and Odej Kao. Anomaly detection from system tracing data using multi-modal deep learning. In *2019 IEEE 12th International Conference on Cloud Computing (CLOUD)*, pages 179–186, 2019. doi: 10.1109/CLOUD.2019.00038.
- Huida Qiu, Yan Liu, Niranjana A Subrahmanya, and Weichang Li. Granger causality for time-series anomaly detection. In *2012 IEEE 12th international conference on data mining*, pages 1074–1079. IEEE, 2012.
- Juan Qiu, Qingfeng Du, Kanglin Yin, Shuang-Li Zhang, and Chongshu Qian. A causality mining and knowledge graph based method of root cause diagnosis for performance anomaly in cloud applications. *Applied Sciences*, 10(6), 2020. ISSN 2076-3417. doi: 10.3390/app10062166. URL <https://www.mdpi.com/2076-3417/10/6/2166>.
- Hansheng Ren, Bixiong Xu, Yujing Wang, Chao Yi, Congrui Huang, Xiaoyu Kou, Tony Xing, Mao Yang, Jie Tong, and Qi Zhang. Time-series anomaly detection service at microsoft. In *Proceedings of the 25th ACM SIGKDD International Conference on Knowledge Discovery & Data Mining, KDD ’19*, page 3009–3017, New York, NY, USA, 2019. Association for Computing Machinery. ISBN 9781450362016. doi: 10.1145/3292500.3330680. URL <https://doi.org/10.1145/3292500.3330680>.

- Lukas Ruff, Robert Vandermeulen, Nico Goernitz, Lucas Deecke, Shoaib Ahmed Siddiqui, Alexander Binder, Emmanuel Müller, and Marius Kloft. Deep one-class classification. In Jennifer Dy and Andreas Krause, editors, *Proceedings of the 35th International Conference on Machine Learning*, volume 80 of *Proceedings of Machine Learning Research*, pages 4393–4402. PMLR, 10–15 Jul 2018. URL <https://proceedings.mlr.press/v80/ruff18a.html>.
- Bernhard Schölkopf, Robert C Williamson, Alexander J Smola, John Shawe-Taylor, John C Platt, et al. Support vector method for novelty detection. In *NIPS*, volume 12, pages 582–588. Citeseer, 1999.
- Kihyuk Sohn, Chun-Liang Li, Jinsung Yoon, Minho Jin, and Tomas Pfister. Learning and evaluating representations for deep one-class classification, 2021.
- Xiuyao Song, Mingxi Wu, Christopher Jermaine, and Sanjay Ranka. Conditional anomaly detection. *IEEE Transactions on Knowledge and Data Engineering*, 19(5):631–645, 2007. doi: 10.1109/TKDE.2007.1009.
- Ya Su, Youjian Zhao, Chenhao Niu, Rong Liu, Wei Sun, and Dan Pei. Robust anomaly detection for multivariate time series through stochastic recurrent neural network. In *Proceedings of the 25th ACM SIGKDD International Conference on Knowledge Discovery & Data Mining*, KDD ’19, page 2828–2837, New York, NY, USA, 2019a. Association for Computing Machinery. ISBN 9781450362016. doi: 10.1145/3292500.3330672. URL <https://doi.org/10.1145/3292500.3330672>.
- Ya Su, Youjian Zhao, Chenhao Niu, Rong Liu, Wei Sun, and Dan Pei. Robust anomaly detection for multivariate time series through stochastic recurrent neural network. In *Proceedings of the 25th ACM SIGKDD International Conference on Knowledge Discovery & Data Mining*, KDD ’19, page 2828–2837, New York, NY, USA, 2019b. Association for Computing Machinery. ISBN 9781450362016. doi: 10.1145/3292500.3330672. URL <https://doi.org/10.1145/3292500.3330672>.
- Jihoon Tack, Sangwoo Mo, Jongheon Jeong, and Jinwoo Shin. Csi: Novelty detection via contrastive learning on distributionally shifted instances. In H. Larochelle, M. Ranzato, R. Hadsell, M. F. Balcan, and H. Lin, editors, *Advances in Neural Information Processing Systems*, volume 33, pages 11839–11852. Curran Associates, Inc., 2020. URL <https://proceedings.neurips.cc/paper/2020/file/8965f76632d7672e7d3cf29c87ecaa0c-Paper.pdf>.
- Aaron van den Oord, Yazhe Li, and Oriol Vinyals. Representation learning with contrastive predictive coding, 2019.
- Li Wu, Jasmin Bogatinovski, Sasho Nedelkoski, Johan Tordsson, and Odej Kao. Performance Diagnosis in Cloud Microservices using Deep Learning. In *AIOPS 2020 - International Workshop on Artificial Intelligence for IT Operations*, Dubai, United Arab Emirates, December 2020. URL <https://hal.inria.fr/hal-02948735>.
- Renjie Wu and Eamonn Keogh. Current time series anomaly detection benchmarks are flawed and are creating the illusion of progress. *IEEE Transactions on Knowledge and Data Engineering*, page 1–1, 2021. ISSN 2326-3865. doi: 10.1109/tkde.2021.3112126. URL <http://dx.doi.org/10.1109/TKDE.2021.3112126>.
- Qizhe Xie, Zihang Dai, Yulun Du, Eduard Hovy, and Graham Neubig. Controllable invariance through adversarial feature learning. In *Proceedings of the 31st International Conference on Neural Information Processing Systems*. Curran Associates Inc., 2018.
- George Zerveas, Srideepika Jayaraman, Dhaval Patel, Anuradha Bhamidipaty, and Carsten Eickhoff. A transformer-based framework for multivariate time series representation learning. In *Proceedings of the 27th ACM SIGKDD Conference on Knowledge Discovery and Data Mining*, KDD ’21, page 2114–2124, New York, NY, USA, 2021. Association for Computing Machinery. ISBN 9781450383325. doi: 10.1145/3447548.3467401. URL <https://doi.org/10.1145/3447548.3467401>.

A Additional Dataset Details

Synthetic data We generate two environmental signals (x_1 and x_2), as well as two system signals (y_1 , and y_2) according to the following set of equations.

$$x_1(x) = \sin\left(\frac{x}{275} - 50\right) + \sin\left(\frac{x}{200}\right) + \epsilon_1 \sim \mathcal{N}(0, 0.05) \quad (8)$$

$$x_2(x) = \sin\left(\frac{x}{100}\right) + \epsilon_2 \sim \mathcal{N}(0, 0.1) \quad (9)$$

$$y_1(x) = x_1(x) + \epsilon_3 \sim \mathcal{N}(0, 0.1) \quad (10)$$

$$y_2(x) = x_1(x) + \frac{x_2(x)}{2} - 2 + \epsilon_4 \sim \mathcal{N}(0, 0.08) \quad (11)$$

Turbine While the turbine dataset consists of 82 distinct time series, our experimentation only operates on a subset of these series. In particular, after preprocessing, we select ambient wind speed (`Amb_WindSpeed_Avg`, `Amb_WindSpeed_Est_Avg`), ambient wind direction (`Amb_WindDir_Relative_Avg`, `Amb_WindDir_Abs_Avg`), and ambient temperature (`Amb_Temp_Avg`), as our environmental variables and generator rotational speed (`Gen_RPM_Avg`), generator power output (`Prod_LatestAvg_TotActPwr`), and two internal temperature sensors (`Gear_Bear_Temp_Avg`, `Hyd_Oil_Temp_Avg`) as our system variables. We select these variables since they do not contain missing values and are easy to interpret. Our core experiments are based on data from the 2016 data set.

Pendulum We simulated synthetic data of a pendulum including friction and control signals (rotational acceleration) following the setup in [Kurle et al. \(2020\)](#). For simulating the ODE, we used the 4-th order Runge-Kutta method. Noisy control signals were sampled from an Ornstein-Uhlenbeck process, where the location of the stationary Gaussian distribution follow a sine signal.

B More Experimental Details

B.1 Hyperparameters

We train all embedding-based methods outlined in Table 2 using batches of size 16 and a learning rate of $1.9 \cdot 10^{-3}$ for 50 epochs. The trained TCN encoder model uses 32 channels, a kernel size of 3 and is comprised of 10 causal convolution blocks. The embedding size is dynamically determined based on the length of the time series (l) and the number environmental and system dimensions (d_{exog} and d_{endog}) as follows: $l \cdot d_{\text{exog}} \cdot d_{\text{endog}} \cdot 0.1$. The negative and positive selection windows mapping into the embedding space are chosen at random locations and are $l \cdot 0.2$ long. Residuals for all residual-based approaches are obtained using the `MLPRegressor` class from `sklearn` with out-of-the box parameters. `Catch22` and `OmniAnomaly` are also run using default parameters.

B.2 Qualitative Results

Figure 4 depicts the effect of isolating intrinsic anomalies via a predictive network on Synthetic data. In Figures 5, we show the effect of learning embeddings on the residuals vs on the actual values. Figure 7 shows qualitatively that we need to modify off-the-shelf time series embeddings in order to be able to isolate intrinsic anomalies. Similar results are available also for the Turbine dataset in Figures 8 and 9. Figure 6 show that purely residual-based approaches can fail in more complex prediction scenarios.

B.3 Quantitative Results

Embedding Space Distances We provide more fine-grained results for the embedding space distance experiment in Table 6.

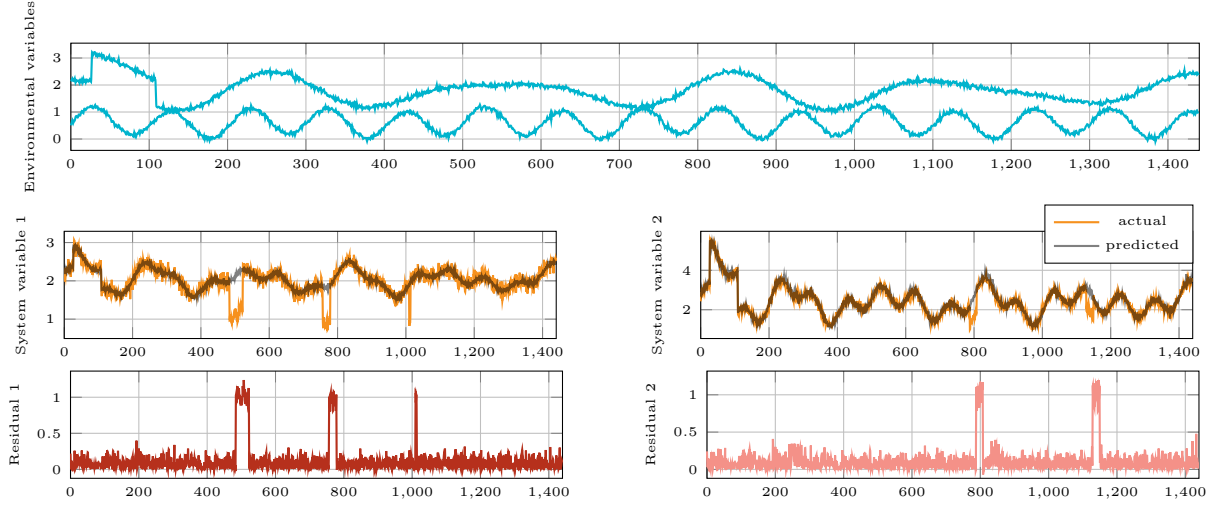


Figure 4: The obtained residuals based on the Synthetic dataset. The top panel shows two distinct environmental variables. For the most part, both series follow a smooth seasonal pattern. The first series shows a noticeable extrinsic anomaly at the beginning of the series. In the middle panel, we depict two endogenous variables along with their predictions. Since the environmental variables do give us some information about the presence of an extrinsic anomaly, we can easily predict a similar anomaly for the system variables. However, each system variable exhibits additional anomalies that are deviating from typical expected behaviour. Considering the residuals in the bottom panel, we can see that the residuals only show these intrinsic anomalies but disregard the predictable extrinsic anomaly at the start.

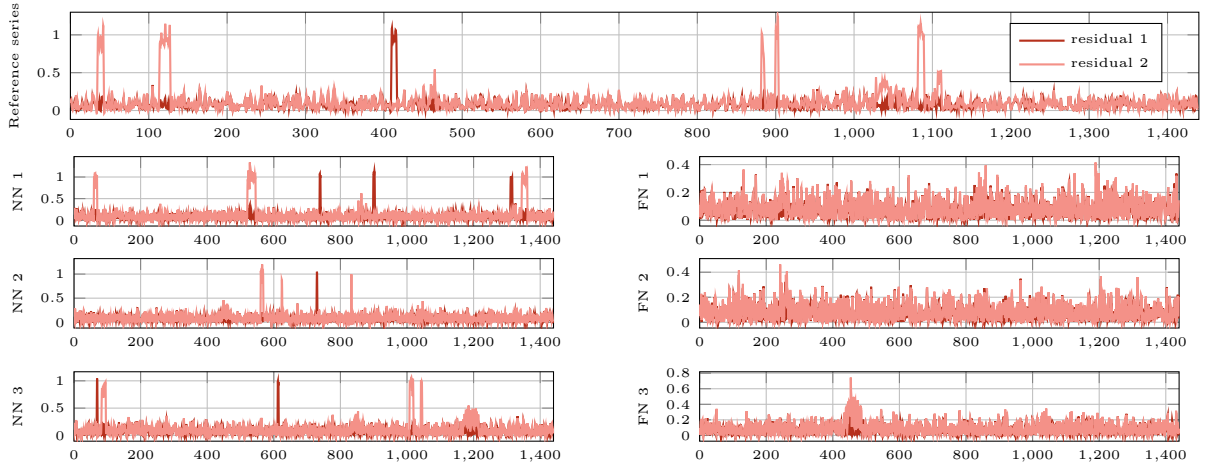


Figure 5: Nearest-neighbor analysis of **ResEmbRegr** for the Synthetic dataset. The top panel depicts an anomalous reference series showing the two residual series, both of which exhibit anomalous behaviour as indicated by the residual spikes. By considering the nearest (NN) and farthest (FN) neighbour series in the embedding space, we can visually inspect the embedding quality. The left panel shows the 3 nearest neighbour series. Clearly, these series align with the reference series since the same spiking pattern in both residuals is present. Considering the farthest neighbours in the right panel, we see that both residual series are noisy without showing pronounced peaks.

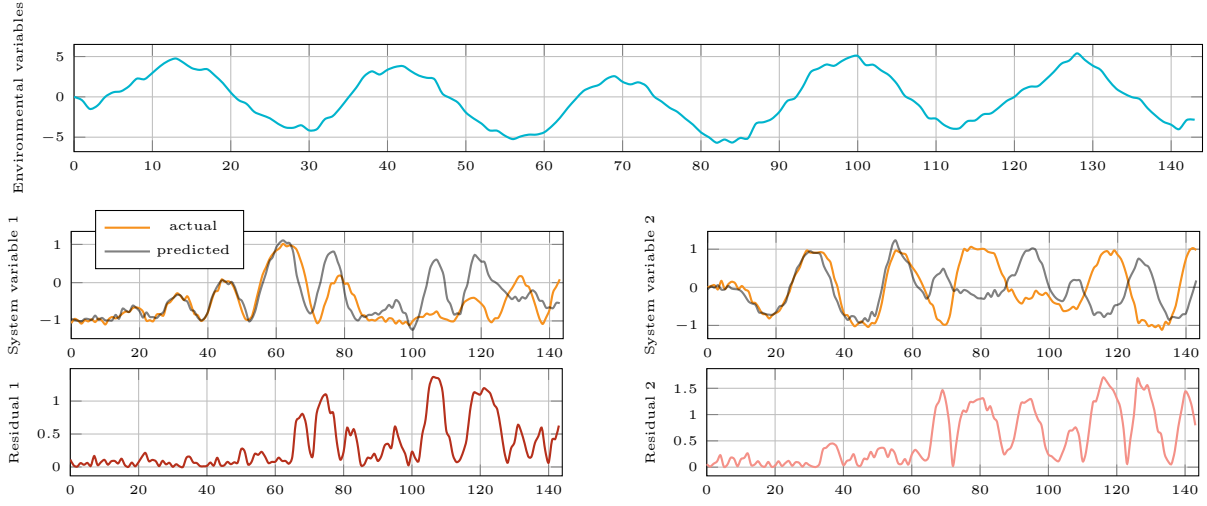


Figure 6: The obtained residuals based on the Pendulum dataset. For this data set, we show the control signal in blue (top panel) and see that we cannot predict the system variables well with an instant-effect, multi-variate regression.

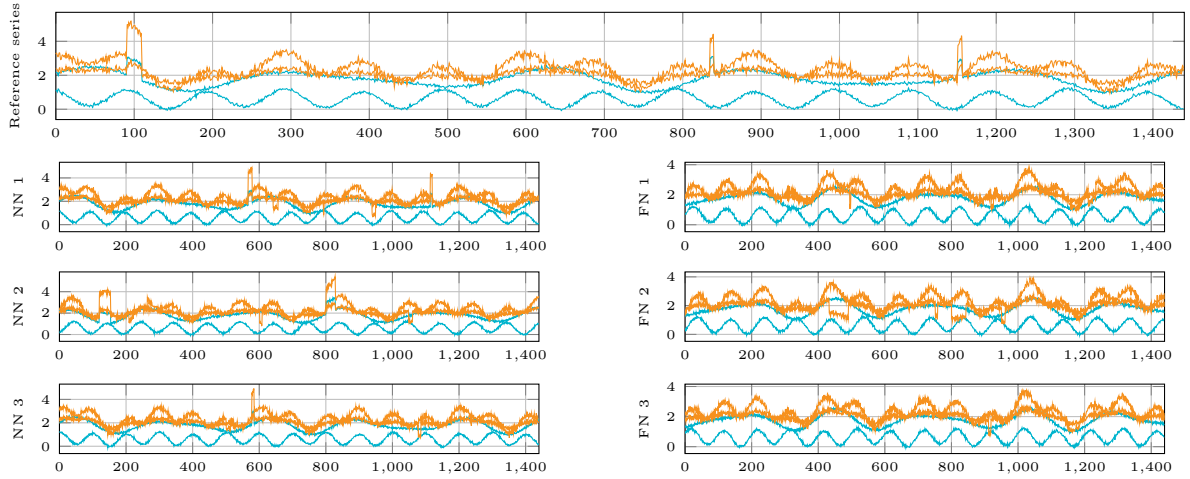


Figure 7: Nearest-neighbor analysis of **BasicEmb** for the Synthetic dataset. The top panel depicts a reference series consisting of both environmental and system signals. The system series do not contain any intrinsic anomalies. In contrast to Figure 5, there is no agreement in the nearest neighbors, as the embedding is unable to pick up on the separation into extrinsic anomalies and intrinsic anomalies.

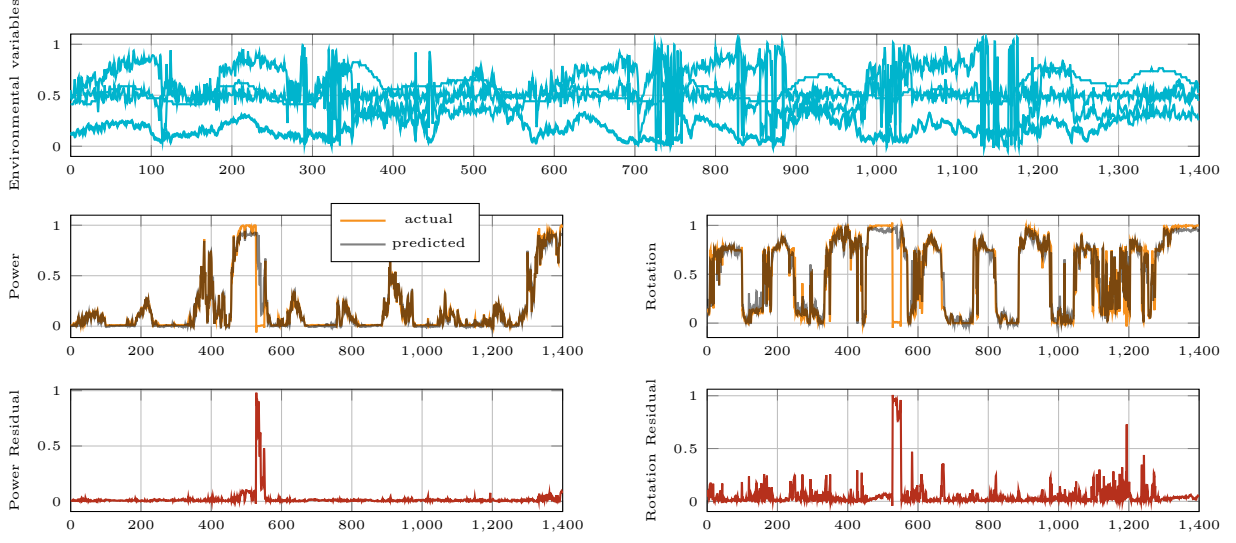


Figure 8: The obtained residuals based on the Turbine dataset. Similar to Figure 4.

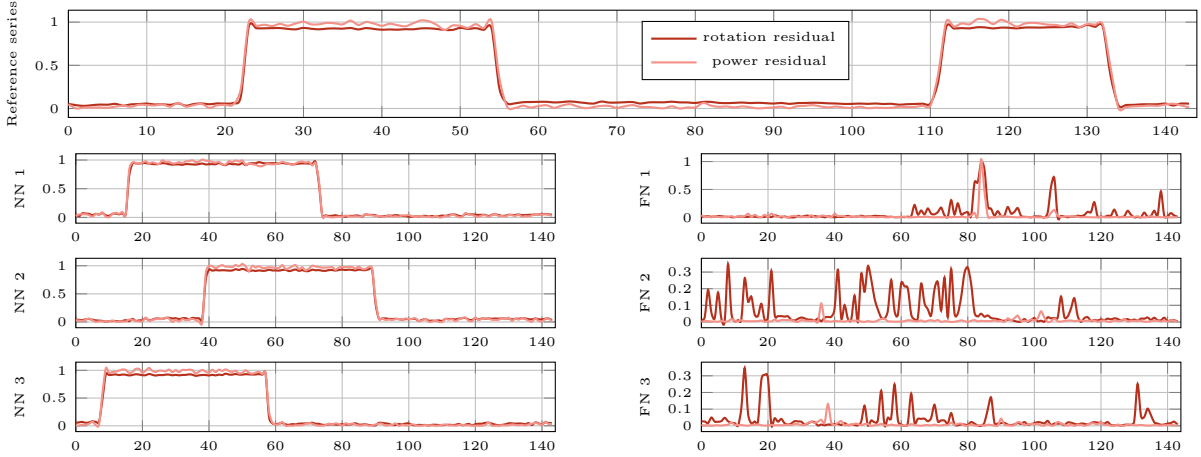


Figure 9: Nearest-neighbor analysis of ResEmbRegr for the Turbine dataset. Similar to Figure 5

Table 5: Sensitivity study on the Synthetic dataset for **EnvInvEmb**. Dependency-breaking negative examples alone ($\lambda = 0$) already provide strong performance and adding adversarial training with a carefully chosen $\lambda = 10^{-3}$ further improves results.

λ	0	10^{-5}	10^{-4}	10^{-3}	10^{-2}	10^{-1}	1
AUROC	0.85 (± 0.12)	0.69 (± 0.15)	0.86 (± 0.06)	0.94 (± 0.03)	0.84 (± 0.14)	0.58 (± 0.09)	0.55 (± 0.07)
F1	0.96 (± 0.03)	0.92 (± 0.04)	0.96 (± 0.02)	0.99 (± 0.01)	0.97 (± 0.03)	0.87 (± 0.04)	0.86 (± 0.04)

The importance of λ We perform an ablation study to determine the influence of trading off the contrastive loss with the adversarial environment-invariance loss in (7), denoted by λ . The results in Table 5, demonstrate that (i) our particular choice of negative examples already provide a strong degree of environment invariance ($\lambda = 0$); and that (ii) these results can be further improved by a careful weighting of the adversarial component. Overall, $\lambda = 10^{-3}$ gives the strongest results, which we also use in our main experimental results in Table 2.

Table 6: Distance results on the anomaly detection task with 5 random seeds. Distances to the correct class (Corr) should be small while distances to the incorrect class (Incorr) should be large. We prefer approaches with a large gap between the mean correct distance and the mean incorrect distance.

Dataset	BasicEmb			ResEmbRegr			EnvInvEmb		
	Corr	Incorr	Gap	Corr	Incorr	Gap	Corr	Incorr	Gap
Synthetic	0.483 (± 0.249)	0.534 (± 0.257)	0.051 (± 0.041)	0.634 (± 0.216)	1.284 (± 0.122)	0.641 (± 0.314)	0.034 (± 0.012)	1.978 (± 0.029)	1.944 (± 0.039)
DevOps	0.918 (± 0.038)	0.932 (± 0.034)	0.446 (± 0.059)	0.942 (± 0.016)	0.977 (± 0.020)	0.433 (± 0.074)	0.043 (± 0.133)	0.529 (± 0.130)	0.486 (± 0.178)
Pendulum	0.691 (± 0.037)	1.137 (± 0.076)	0.014 (± 0.006)	0.679 (± 0.036)	1.112 (± 0.065)	0.035 (± 0.008)	0.215 (± 0.178)	0.437 (± 0.346)	0.012 (± 0.007)
Turbine	0.927 (± 0.024)	1.002 (± 0.022)	0.075 (± 0.007)	0.691 (± 0.186)	1.010 (± 0.272)	0.319 (± 0.103)	0.065 (± 0.079)	0.516 (± 0.161)	0.450 (± 0.085)